Proceedings of the 7th International Conference on Materials Chemistry and Environmental Engineering
DOI: 10.54254/2755-2721/2027.38443

How Does the Inter-Rib Angle Affect the Lifting Angle of an Earwig-Inspired Folding Structure — An Experimental Study Using Paper Models

Tianyu Li

Shunde Desheng School, Ronggui, China
13336422529@163.com

Abstract. This study focuses on the internal angle of the earwig wing paper model, a biologically inspired model that has been widely studied. The mechanism inspired by the earwig wing demonstrates unique crease pattern that contains a double bistable state. In total, we made 10 different paper models, each with a different internal angle. The range of the internal angle is from 40 to 130 degrees to investigate the effect of changing the internal angle on the lifting angle of the paper earwig model. The tool used to obtain the lifting angle measurement is ImageJ. During the experiment, Section1 was fully folded, and a standard horizontal line was put for reference, then the Section 2 lifted up automatically. Our data shows that when $\theta \leq 60°$the lifting angle shows downward trend, and when $60° < \theta \leq 90°$, and when $90° < \theta$ the lifting angle start to decrease again. This study suggests that the reason of this might because the changing of θ al so change the proportion of length of mountain and valley line.

Keywords: earwig wing, Bio-inspired design, origami, folding kinematics, deployable structure

1. Introduction

The deployable structures are movable structures that are able to alter their geometric shapes to satisfy different requirements. These deployable structures surround our lives. They range from everyday items such as deployable smartphone screens and umbrellas to more advanced aerospace applications. The technology of "folding and unfolding" is demonstrated in various areas. For example, in outer-space missions, solar power systems on satellites, antennas, and robotic arms. Those structures are increasingly larger. The purpose of deployable structures is to be stored in a relatively smaller space and then expand into a larger area. This makes transportation and launching processes more convenient and effective. Some engineers extract features from creatures in nature, particularly insects. These biological features have inspired a range of engineered structures. For example, ants (Formicidae) use a highly efficient gait pattern to move stably across uneven terrain. Bees (Apis mellifera) offer insights into aerodynamic efficiency and wing–wake interactions, while butterflies (Morpho spp) have revealed highly ordered photonic crystal arrangements that produce structural coloration without pigments [1]. The creases and structures from plants, insects, and

© 2026 The Authors. This is an open access article distributed under the terms of the Creative Commons Attribution License 4.0 (https://creativecommons.org/licenses/by/4.0/).

DOI: 10.54254/2755-2721/2027.38443

animals are increasingly applied in aerospace applications due to their high compactness. For example, beetles. Regarding folding methods, beetles exhibit the most diverse variations, but the most compact folding can be observed in earwig wings [2](Fig. 1A). The special fan-shaped crease pattern allows the ribs to move closer to the centre, which grants them high compactness in wing stowage among insects. The folding ratio reaches 1:10 in the European earwig (Forficula auricularia) and 1:18 in the lesser earwig (Labia minor) [3, 4]. Moreover, the earwig wing exhibits a bistable state, which does not require any extra energy to switch rapidly between the folded and unfolded states, contributed by its soft membrane and elastic resilin. Earwig wings have been researched for a long time. In 2020, Saito and his group members used X-ray scanning to analyse the internal structure of the earwig wing, and thus proposed a geometric design based on a "plane-foldable" method [5](Fig. 1B). In 2022, Salvador and his group members combined traditional origami and resilin to form a multistable and reprogrammable origami structure, which can change its state through external factors such as temperature [6]. In 2025, Blinder and his group members introduced a set of mathematical tools to simulate the dynamics of insect wing folding based on the MuJoCo physics engine and Python. They abstracted the wing into a bar-hinge linkage [7]. Those previous studies mainly focus on understanding the biological folding mechanism of earwig wings and reproducing their folding crease lines and rules for engineering applications. These studies have successfully demonstrated how earwig-inspired folding patterns can achieve a high compactness ratio and have provided design methods for bio-inspired deployable structures. However, relatively little attention has been given to how variations in geometric parameters within the folding pattern influence the kinematic behaviour of the structure. In particular, the effect of the inter-rib angle on the lifting angle of the second section during folding has not been systematically investigated. Here, this study experimentally examines the relationship between the inter-rib angle and the lifting angle of Section 2 (Fig. 1C) when the structure is undergoing the folding process. By constructing paper-based physical models with different inter-rib angles while keeping the remaining geometric parameters constant, this study seeks to examine the relationship between rib geometry and folding behaviour. The findings are expected to improve the understanding of the geometric principles governing earwig-inspired folding mechanisms and provide useful insights for the design of future bio-inspired deployable structures.

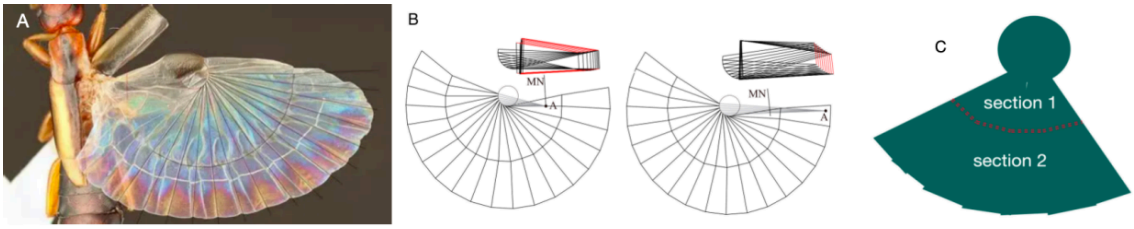


Figure 1. (A) The demonstration of the earwig wing. (B) The abstract geometric structure of the earwig wing and folded state from Saito et al. (C) The demonstration of the section of the earwig wing

2. Experimental methodology

This section describes the experimental methodology used in the design, measurement, and folding to investigate the effect of changing the inter-rib angle on the lifting angle of Section 2. The experimental procedure includes two main stages: the construction of paper-based models with different inter-rib angles, and the measurement of the lifting angle using a digital image processing tool.

DOI: 10.54254/2755-2721/2027.38443

2.1. Experimental approach

The folding pattern proposed by Saito et al. [5] was adopted as the basis of the experimental models. The inter-rib angle, θ , defined as $\angle H_1V_1F_2$, was selected as the independent variable(Fig2 A). The angle was varied from 40 ° to 130 ° in 10 ° increments, resulting in ten different paper-based models. For each model, θ was the only deliberately varied geometric parameter, while the remaining parameters were kept constant. All models were constructed using the same A4 paper, with the same number of ribs and the same Section 1 geometry based on the radial reference geometry described by Saito et al. Section 2 was constructed by extending the corresponding lines of Section 1 by a fixed length of 5 cm. This 5 cm length was kept constant for all models. After the inter-rib angle was set, the remaining points and rib positions were allowed to change naturally according to the resulting geometric configuration. No additional geometric adjustments were made to compensate for changes in θ . The mountain and valley crease pattern was kept identical for all models. At each folding node, the three designated creases were folded as mountain folds and the remaining crease as a valley fold, with the mountain and valley assignments alternating at successive nodes according to the selected origami folding pattern. The crease lines were marked on the paper before folding, but the models were not pre-creased(Fig. 2B). Each model was folded directly according to the designated mountain and valley pattern(Fig. 2C). Folding was stopped when Section 1 reached its fully folded configuration. At this stage, Section 2 lifted away from the horizontal plane, producing the lifting angle investigated in this study. The lifting angle of Section 2 was defined as the angle between Section 2 and the horizontal reference line formed by the fully folded Section 1(Fig. 2D). The final configuration of each model was photographed with Section 2 facing the camera to reduce the effect of viewing direction on the measured angle. One model was produced for each inter-rib angle, giving a total of ten experimental models. The resulting lifting-angle data were subsequently compared across the different inter-rib angles to investigate the relationship between rib geometry and the folding behaviour of the second section.

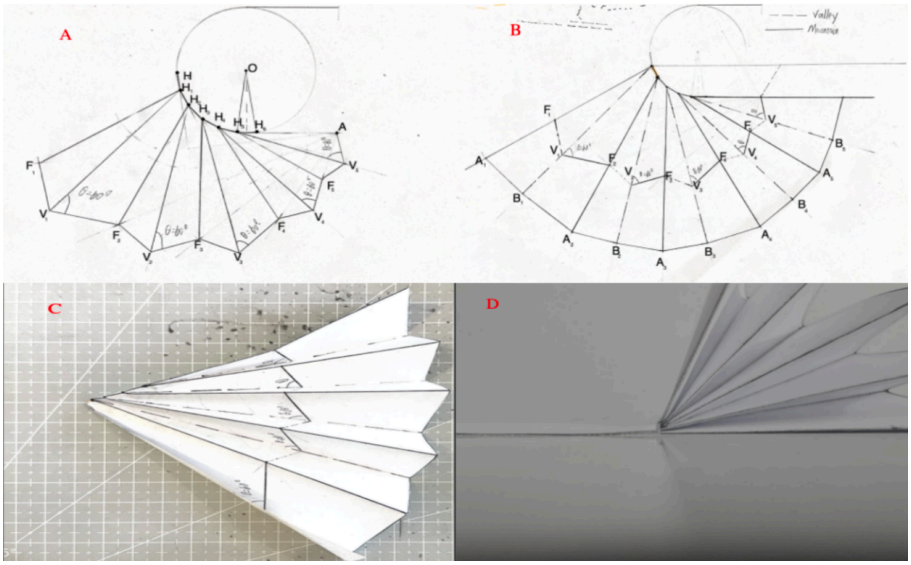


Figure 2. (A)The geometric drawing and folded paper demonstration. (B)Construction of the starting geometric element and section 1(circle O , point A, and internal rib angle θ). (C)The entire origami drawing of the earwig wing where θ=60° and crease pattern folded according to crease pattern. (D)Lifting angle measured when section 1 is fully folded. (E)Demonstration of use of ImageJ to process data

DOI: 10.54254/2755-2721/2027.38443

2.2. Image processing

ImageJ (National Institutes of Health, USA) is an open-source image processing and analysis program widely used in scientific research [8]. It provides a comprehensive set of tools for standard image operations (e. g., scaling, contrast adjustment, background subtraction) and quantitative measurements, including distance, area, and angle calculations from user-defined selections(Fig. 3A). In this study, ImageJ was used to measure the lifting angle of Section 2 from the photographs of each folded paper model. The angle measurement tool was then employed as follows: a horizontal reference line was drawn along the fully folded Section 1, and a line was drawn along the flat surface of Section 2 from its root to its distal end(Fig. 3B). Then the software automatically calculated the angles between these two lines, which were recorded as the lifting angle(Fig. 3C). The measurement was repeated three times for each photograph, and the average value was used to minimise errors. The whole measurement processes applied consistently across all the ten models, ensuring comparability of the resulting data.

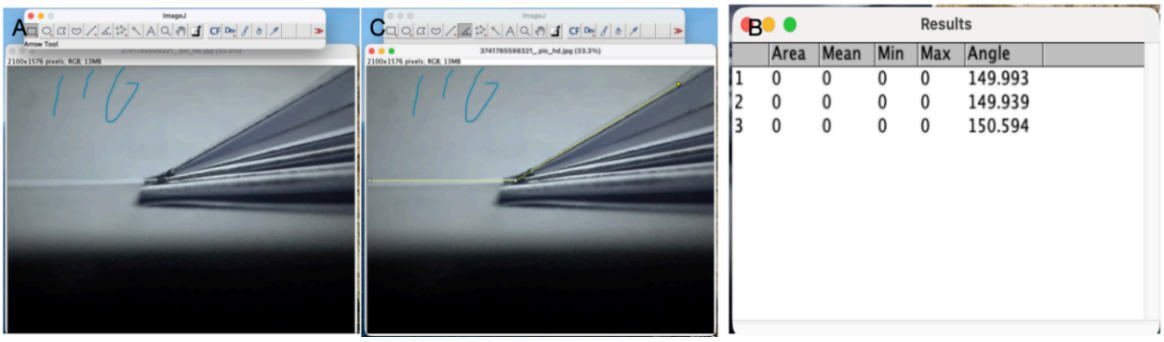


Figure 3. (A)The demonstration of the initial page after inserting pictures. (B)The demonstration of measurement; the yellow line is used to measure the angle. (C)The table showing the measurement of lifting angle

3. Experimental result

This section presents the results of foldability verification and angle measurements of ten paper-based models that have different inter-rib angles. This section also shows the demonstration of the folding process. These results are presented to verify the foldability of the proposed folding pattern and to demonstrate the effect of changes in inter-rib angle on the lifting angle of Section 2.

3.1. Folding-ability verification

To ensure all the modules can really be folded, three criteria are established from origami kinematics: Kawasaki's theorem, Maekawa's theorem, and single-vertex mobility analysis. According to Kawasaki's theorem, a vertex crease pattern is only flat foldable if the sum of alternated angles around the vertex equals to 180 ° .

In this study, two types of vertices were examined. The first type includes the central nodes H_1,H_2,H_3. . . . . to H_5 along the primary folding axis, which multiple ribs converge. The second type comprises the vertices formed by the independent variable angles, the V and F points(Fig. 2A). For each vertex, the sums of alternating angles were calculated to confirm that those module patterns are all flat-foldable. Maekawa's theorem was applied to verify that the mountain–valley assignment at each vertex is correct. This theory states that for a flat-foldable vertex, the difference between the

DOI: 10.54254/2755-2721/2027.38443

number of mountain creases and valley creases must be 2, as shown in Equation 2. As illustrated in Fig. 4, each vertex in the current folding pattern satisfies this condition, confirming that the assignment of mountain and valley folds is kinematically valid. Moreover, the kinematic mobility of the structure was examined using the single-vertex degree-of-freedom condition, according to Equation 3, where N is the number of crease lines meeting at the vertex [9]. This analysis determines whether the folding motion is uniquely constrained. For the present patterns, all vertices satisfy the mobility condition, indicating that the structure is neither over-constrained nor under-constrained. The results of these three analyses—Kawasaki's theorem, Maekawa's theorem, and DOF assessment—are summarised in Table [1] for all models.

$$\alpha + \beta = \varphi + \phi = 180^{\circ} \tag{1}$$

$$|M - V| = 2 \tag{2}$$

$$DOF = N - 3 \tag{3}$$

Table 1. Summary of geometric foldability criteria for all models

Criterion	Result	Remark
GOF	1	N=4
Kawasaki's theorem	Satisfied	each node Alternate angle sum = 180° for all vertices
Maekawa's theorem	Satisfied	at each vertex

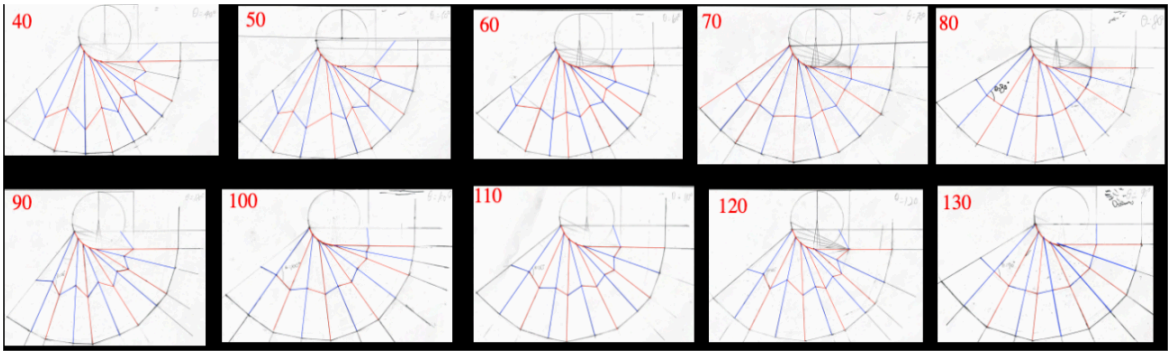


Figure 4. Demonstration of origami pattern of fix θ models from 40° to 130° and it's mountain and valley distributions, red for mountain lines, blue for valley lines

3.2. Demonstration of folding process

The model with θ = 90° was selected to demonstrate the whole folding process and the resulting configuration. There are two reasons for choosing the θ = 90° model. Firstly, it reaches the peak of the lifting angle data, where the structure reaches its maximum lifting angle. Secondly, this geometry most close to the original earwig wing folding pattern reported by Saito et al , making it a suitable reference for demonstrating the folding behaviour. The crease pattern of the θ = 90° model is drawn according to the geometric parameters described in Section 2. 1. The mountain and valley lines were assigned following the alternated fold pattern, which satisfies both Kawasaki's theorem and Maekawa's theorem as verified in Section 3. 1. 1. The resulting crease patterns show in Fig. 5A. The model was folded progressively from the flat state (Fig. 5B) to a partially folded configuration

DOI: 10.54254/2755-2721/2027.38443

(Fig. 5C), and finally until Section 1 reached its fully folded state. The lifting of Section 2 occurred simultaneously when folding Section 1, indicating that the two sections are kinematically coupled throughout the folding process. It is observed that the creases became less and less resistant, and the resistance at the central node gradually diminished after numerous fold these might different according to different materials used. To maintain the fully folded configuration during measurement, Section 1 was secured using transparent adhesive tape and paper (Fig. 5D). As folding progressed, it is observed that Section 2 is lifting away from the horizontal plane. This lifting behaviour is attributed to the mechanical interaction between adjacent panels and ribs near the central node H, V, and F, where the convergence of multiple creases generates both in-plane and out-of-plane forces that drive Section 2 upward (Fig. 5E). A notable geometric feature observed in the fully folded configuration is that at the junction between Section 1 and Section 2, all internal rib lines become collinear and converge into a single vertex at the connection between the two sections. This convergence indicates that the folded geometry reaches a consistent nodal configuration where the folding motion of Section 1 is fully transmitted to the root of Section 2. The lifting angle was measured using the ImageJ procedure described in Section 2. The horizontal reference line was defined along the base of the fully folded Section 1, and the Section 2 line was drawn along its flat surface from the root to the distal end. The measured value for this representative case was approximately 124° (corresponding to a true lifting angle of approximately 56°).

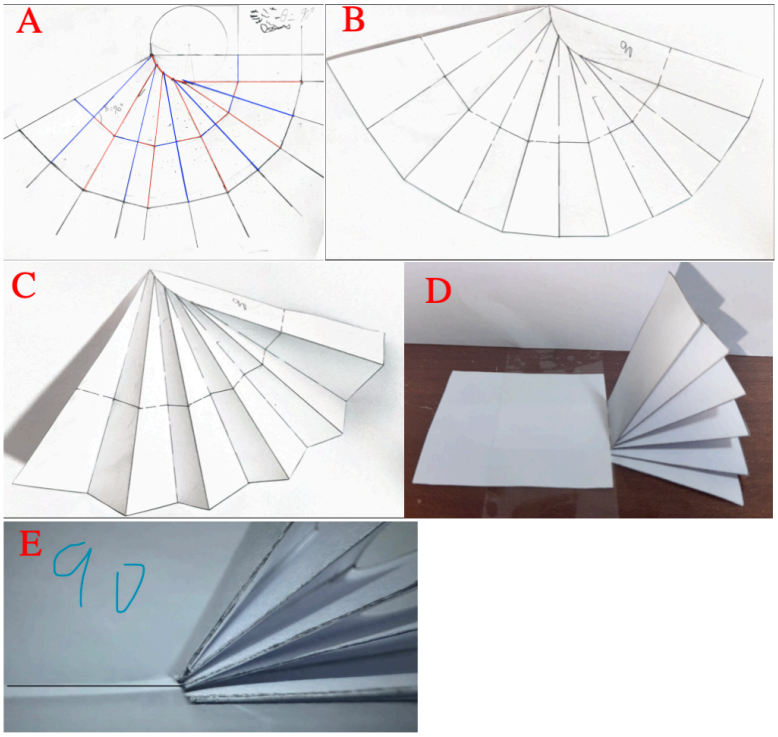


Figure 5. (A)Demonstration of the origami pattern of the earwig wing model whenθ=90°, red is mountain lines, blue is valley lines. (B&C)Showing the model after cutting the extra paper and half-folding according to the origami pattern. (D)Showing how section 1 and the model are immobilized and section 2 lifts naturally. (E)Demonstration of lifting angle and black reference line

DOI: 10.54254/2755-2721/2027.38443

3.3. Result: lifting angle measurements

The lifting angles measured from all 10 models are presented in Table 2. The measured values represent the angle between Section 2 and the horizontal reference line defined by the fully folded Section 1. The lifting angle is calculated as 180° minus the measured value. Each model took approximately 30 minutes to fold, including pattern tracing, cutting, creasing, and final configuration setup. This experiment required a high level of similarity between each model, as the crease pattern remained identical and only the inter-rib angles θ is varied. No model was damaged or discarded during fabrication(Fig. 6). The data exhibits a clear non-monotonic trend(Fig. 7). As the inter-rib angles increase, the lifting angles vary across the tested range, with a distinct turning point observed when θ = 90° and θ = 60°, where the structure reaches its maximum and minimum true lifting angle. It is clear that θ angle between 40 ° to 60 ° shows a downward trend of lifting angle, then it experiences a dramatic increase and stand at the peak which when θ = 90° and lifting angle equal 55. 7°. After this, the angle drops significantly and shows a continuous downward trend; thus, a prediction is generated that the lifting angle will keep declining as θ keeps increasing after θ = 90°. The specific data are shown in Table 2. Moreover to assess repeatability, three selected angles were folded and measured a second time there 60 ° , 90 ° and 130 ° . In addition to the measured lifting angles, a qualitative observation was made regarding the folded footprint of Section 2. When Section 2 was fully folded down onto the horizontal plane, which fully covers Section 1, its coverage area shifted with changing inter-rib angles. This shift is attributed to the rotation of the rib directions as θ varies, which alters the spatial orientation of Section 2 relative to Section 1. For each photograph, the angle was measured three times using ImageJ, and the average value was recorded to reduce random errors. The primary sources of measurement error are considered to be slight deviations in the actual rib angles during manual folding, which may not perfectly match the intended θ values, and the manual placement of reference lines in ImageJ, which introduces some degree of subjectivity.

Table 2. The included angle(i. e. lifting angle) between section2 and horizontal table surface(1. d. p)

Number	θ angle °	Lifting angle
1	40 °	45. 2 °
2	50 °	40. 8 °
3	60 °	36. 9 °
4	70 °	44. 0 °
5	80 °	53. 5 °
6	90 °	55. 7 °
7	100 °	36. 1 °
8	110 °	28. 5 °
9	120 °	28. 1 °
10	130 °	20. 3 °

DOI: 10.54254/2755-2721/2027.38443

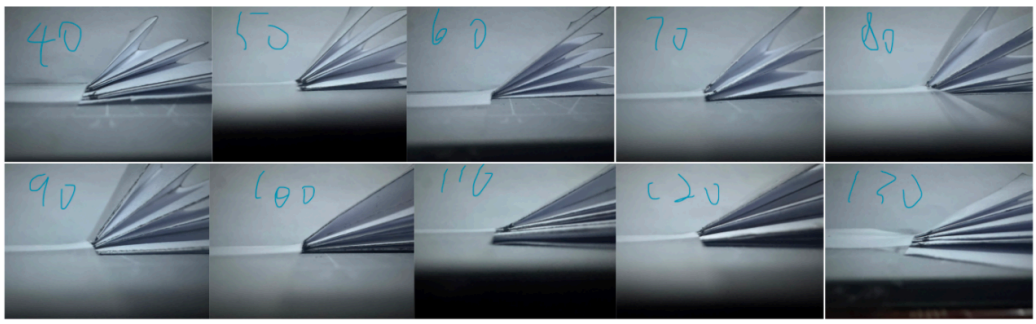


Figure 6. Demonstration of all ten models during measurement

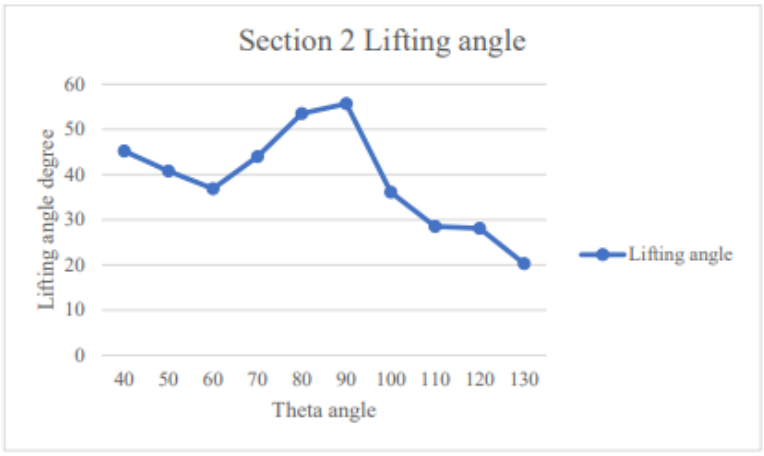


Figure 7. Demonstration of the line graph and trend of data

4. Analyzing

When drawing the crease pattern of the origami earwig wing, all ribs HA and HB are exactly the same length, which means that the rib lengths and the area distribution are identical across models, except for the angle ∠HVF(Fig. 2). It is observed that although ribs HA and HB do not physically converge at a single point in the flat pattern, they still spread outwards during the folding process. In the experiment, when Section 1 is fully folded, the rib lines eventually converge into a single point. This forms a configuration structurally similar to that of an accordion fan(Fig. 8A & B).

This leads to the hypothesis that the force that spreads Section2 may have the same energy source as a fan structure(Fig. 7C). The mechanical work is done when a hand applies an external force to the folding structure. This input energy is stored within the paper material as elastic potential energy, more specifically along the creases and curved panels. When the structure is released, the stored energy is able to drive rotational motion, causing Section 2 to fold up. Moreover, when the folding force is removed, Section 2 remains in its lifted position rather than returning to the flat state. This indicates that the elastic recovery force is balanced by geometric constraints and frictional contacts. This kind of energy balance explains why the folded configuration is continuously stable without external support. Hence, the theory of accordion fan mechanics can be applied to explain the observed variation in lifting angle. One of the important factors is the proportion of mountain and valley line lengths. While the total lengths of lines HB and HA are kept constant across models, the lengths of HF and HV vary when θ changed (Fig. 4). It is noticed that when $40^\circ < \theta \leq 60^\circ$, the valley lines HV are the longest. When $60^\circ < \theta \leq 90^\circ$, the lengths of HF and HV become more

DOI: 10.54254/2755-2721/2027.38443

evenly matched. When $90^{\circ} < \theta \leq 130^{\circ}$, the mountain lines HF become the longest. This shifting in length proportion directly affects the force transmission path from Section 1 to Section 2. Assuming that the total elastic potential energy stored in paper is comparable across all models. Since the rib spacing, material properties, and folding angle are consistent, the only remaining factor that influences the lifting angle is the proportion between the lengths of HF to FA, and between HV to VB, as well as the relative lengths of the mountain and valley lines. This suggests that the lifting angle is not determined solely by the amount of stored energy, but also by how that energy is distributed and transmitted through the asymmetric fold network. This depends on the balance between mountain and valley line lengths. To prove this, one of the dependent variables is the internal valley rib XY. It is clear that for all folded experimental models, the position of point X remains unchanged, while the position of Y shifts according to the inter-rib angle θ (Fig. 9). So, as Y moves, the area distribution between Section 1 and Section 2 is redistributed. The larger the angle, the larger the area of Section 2, and vice versa. Assuming that Section 1 consists of all the main ribs HV and HF, while Section 2 is only the external extension from Section 1, most of the elastic energy will be stored in Section 1 during folding. Therefore, because most of the energy is stored in Section 1, any geometric change that alters the area distribution between the two sections will affect how that stored energy is transmitted, influencing the resulting lifting angle of Section 2.

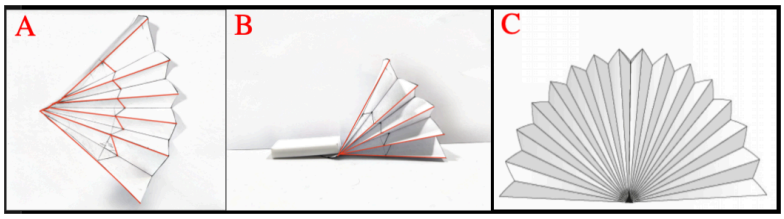


Figure 8. (A) Demonstration of the lateral view of the origami earwig wing; the red lines are mountain lines. (B) Demonstration of lateral view of origami earwig wing, the red lines are mountain, that section1 been folded half until all the rib converge into a same point. (C) Demonstration of accordion fan origami

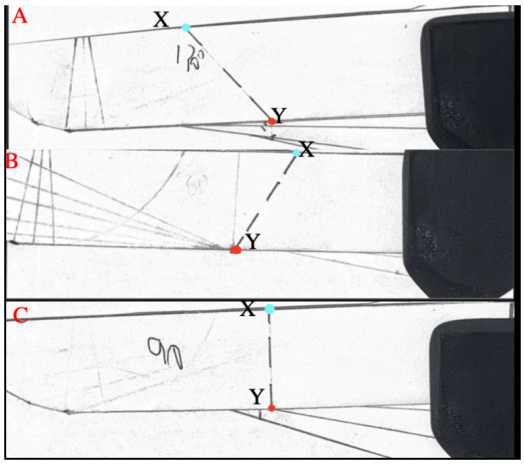


Figure 9. (A) Demonstration of the planform of earwig wing origami when both section 1 and section 2 are horizontally folded and θ=130°. (B) Demonstration of the planform of earwig wing origami when both section 1 and section 2 are horizontally folded and θ=60°. (C) Demonstration of the planform of earwig wing origami when both section 1 and section 2 are horizontally folded and θ=90°

DOI: 10.54254/2755-2721/2027.38443

5. Limitation

In this experiment, some limitations should be known. Firstly, there may affect the accuracy of the crease pattern, and con not be exactly the same as what real insects do. Secondly, the final angle measurements rely on manual line placement, which may be subjective and is sensitive to camera angle and lighting. Moreover, the whole experiment in this paper only use normal A4 paper as the material, which result may changed as material changed. And the modules made for experiments are all small in size, so the data may vary when changing the size.

6. Conclusion

This study investigates the effect of internal rib angle θ on the lifting angle in an earwig-inspired folding structure. In total, 10 paper-based models with different θ angles from 40° to 130° with a 10° increment were tested. All the models have been verified as geometrically foldable using Kawasaki's theorem, Maekawa's theorem, and single-vertex mobility analysis. The lifting angle exhibited a clear non-monotonic trend, with a local maximum at θ = 90° and a minimum at θ = 60°. This variation is attributed to the accordion-like energy storage and release mechanism. The internal rib angle alters the proportion of different rib lengths. Which changing the force transmission path from and finally determining the lifting angle. The experiments were repeated three times to ensure accuracy and show that this test is reproducible. Future work could examine the effects of uneven rib distribution and under different material properties.

Acknowledgement

The author would like to thank Prof. You for his valuable guidance and fruitful discussions throughout the course, and Teaching Assistant Song for his constructive suggestions on improving this work.

References

[1] Abbasi, E. (2025). Biological sensors and bio-inspired technologies: The role of insects in advanced detection systems and robotics. *Discover Applied Sciences, 7*, 503, pp. 5-6. https://doi.org/10.1007/s42452-025-07000-6

[2] Saito, K., Kitajima, C., Nishi, K., & Sato, J. (2026). Earwig fan-inspired deployable structures. In G. Lu, Z. You, & M. Assis (Eds.), *Origami8, Volume II: Proceedings of the 8th International Meeting on Origami in Science, Mathematics and Education (8OSME), Lecture Notes in Mechanical Engineering* (pp. 294-295). Springer. https://doi.org/10.1007/978-981-96-8661-2_20

[3] Haas, F., Gorb, S., & Wootton, R. J. (2000). Elastic joints in dermapteran hind wings: Material and wing folding. *Arthropod Struct. Dev., 29*. [CrossRef]

[4] Deiters, J., Kowalczyk, W., & Seidl, T. (2016). Simultaneous optimisation of earwig hind wings for flight and folding. *Bio. Open, 25*. [CrossRef]

[5] Saito, K., Pérez-de la Fuente, R., Arimoto, K., Seong, Y. A., Aonuma, H., Niiyama, R., & You, Z. (2020). Earwig fan designing: Biomimetic and evolutionary biology applications. *Proceedings of the National Academy of Sciences, 117*(30), pp. 17699-17704. https://doi.org/10.1073/pnas.2005769117

[6] Rojas, S., Riley, K. S., & Arrieta, A. F. (2022). Multi-stable bio-inspired origami with re-programmable self-folding. *Journal of the Royal Society Interface, 19*(195), 20220426. https://doi.org/10.1098/rsif.2022.0426.

[7] Binder, N., Costi, L., Izzo, D., & Seidl, T. (2026). Quantifying nature's bistability: Simulation of earwig fan folding. *Biomimetics, 11*(1), 9. https://doi.org/10.3390/biomimetics11010009.

[8] Schneider, C. A., Rasband, W. S., & Eliceiri, K. W. (2012). NIH Image to ImageJ: 25 years of image analysis. *Nature Methods, 9*(7), 671–675.

[9] Guest, S. D., & Pellegrino, S. (1994). The folding of triangulated cylinders, part I: Geometric considerations. *Journal of Applied Mechanics, 61*(4), 773–777.